ChemComm

COMMUNICATION

View Article Online
View Journal | View Issue

Cite this: *Chem. Commun.*, 2019, **55**, 4695

Received 8th January 2019,
Accepted 18th March 2019

DOI: 10.1039/c8cc10134e

rsc.li/chemcomm

The two isomers of a cyclometallated palladium sensitizer show different photodynamic properties in cancer cells†

Xue-Quan Zhou, [a] Anja Busemann, [a] Michael S. Meijer, [a] Maxime A. Siegler [b] and Sylvestre Bonnet *[a]

This report demonstrates that changing the position of the carbon–metal bond in a polypyridyl cyclopalladated complex, *i.e.* going from PdL^1 (N^N^C^N) to PdL^2 (N^N^N^C), dramatically influences the photodynamic properties of the complex in cancer cells. This effect is primarily attributed to the significantly difference in absorbance and singlet oxygen quantum yields between the two isomers.

The success of cisplatin, a milestone drug in the treatment of cancers, stimulated the generation of many platinum-based anticancer drugs,[1–3] three of which (carboplatin, oxaliplatin and nedaplatin) are approved worldwide. However, the unselective covalent binding of cisplatin with DNA in cancer cells and healthy cells results in serious side effects and drug resistances, which has encouraged the development of anticancer drugs based on alternative metals.[4–9] In this regard, palladium(II) complexes have been proposed as potential metal-based anticancer drugs for their similar d^8 coordination sphere and square-planar structure, compared to platinum(II) complexes.[10,11] One of them, called padeliporfin or WST11, was recently approved for photodynamic therapy (PDT) of prostate cancer.[12] PDT is a form of light-activated anticancer treatment. It emerges as a more patient-friendly approach due to the controlled toxicity effect and low invasiveness of light irradiation.[13–17] In PDT, a photosensitizing agent (PS) is irradiated by visible light at the tumor site, where it generates cytotoxic reactive oxygen species (ROS), which induces cancer cell death.[18] Polypyridyl metal complexes typically form excellent PDT sensitizers, provided they strongly absorb visible light.[19,20] The light absorption properties of such complexes can be tuned by changing the metal or the ligands. Critically, good photosensitizers should be photostable, which can be achieved using multidentate ligands. The single coordination bonds in multidentate complexes are no stronger than those of monodentate ligands, they are simply less likely to all decoordinate at once.

Recently, bioactive pincer palladium complexes with tridentate N-heterocyclic carbene ligands have been shown to possess stable metal–carbon bonds and tuneable physicochemical properties.[10,21–24] However, intracellular substitution of the remaining monodentate ligands makes their speciation in biological media and mode-of-action complicated to understand. In addition, due to the smaller ionic radius of Pd^{2+} ions, Pd–ligand bonds are longer and more labile than their Pt–ligand analogues,[25] so that anticancer drugs based on palladium(II) are still comparatively rare.[6] To overcome these drawbacks, we investigated the design and properties of palladium(II) PDT sensitizers built from single tetradentate cyclometallating ligands, which are expected to be more stable in biological media compared with the tridentate N-heterocyclic carbene ligands. Cyclometallation was considered for different reasons. Firstly, the strong Pd–C bond can stabilize these compounds in biological media. Secondly, the lower charge introduced by the cyclometallated ligand can improve the lipophilicity and cellular uptake of the metal complexes.[7,26] Finally, the presence of a Pd–C bond should in principle lead to a bathochromic shift of the visible absorption bands of the metal complex, which is key for PDT applications.[27]

In polypyridyl metal complexes, introducing a metal–carbon bond usually generates a series of isomers that might have different properties. Herein we investigated two novel cyclopalladated isomers **PdL^1** (**H$_2$L^1** = *N*-(3-(pyridin-2-yl)phenyl)-[2,2′-bipyridin]-6-amine) and **PdL^2** (**H$_2$L^2** = *N*-(6-phenylpyridin-2-yl)-[2,2′-bipyridin]-6-amine) (Scheme 1a). In **PdL^1**, the Pd–C bond was introduced in a pyridyl group that is adjacent to the non-bonded nitrogen bridge of the ligand, while in **PdL^2** it is introduced in one of the terminal aromatic rings. The ligands **H$_2$L^1** and **H$_2$L^2** were synthesized by Buchwald–Hartwig coupling reactions (Scheme S1 and Fig. S1–S4, ESI†).[28–30] Palladation was achieved in more than 90% yield by reacting the corresponding ligand with palladium(II) acetate in acetic acid (Scheme S1 and Fig. S5–S8, ESI†). Neither ^{1}H NMR (Fig. S5 and S7, ESI†) nor infrared spectroscopy (Fig. S9, ESI†) showed any sign of a protonated

[a] *Leiden Institute of Chemistry, Universiteit Leiden, Einsteinweg 55 2333 CC, Leiden, The Netherlands. E-mail: bonnet@chem.leidenuniv.nl*
[b] *Department of Chemistry, Johns Hopkins University, Maryland 21218, Baltimore, USA*

† Electronic supplementary information (ESI) available: Experimental details, graphical results, and videos. CCDC 1534260. For ESI and crystallographic data in CIF or other electronic format see DOI: 10.1039/c8cc10134e

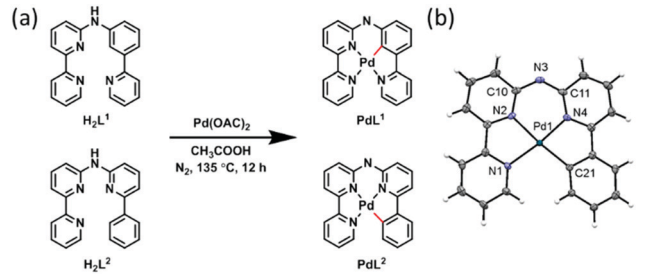

Scheme 1 (a) Synthesis of **PdL^1** and **PdL^2**; (b) displacement ellipsoid plot (50% probability level) of **PdL^2** at 110(2) K (bond distance: Pd–N1 2.060(3) Å, Pd–N2 2.028(4) Å, Pd–N4 1.988(3) Å, Pd–C21 2.017(4) Å); angle: N4–Pd1–C21 81.99(15)°, N4–Pd1–N2 92.66(16)°, C21–Pd1–N2 174.65(18)°, N4–Pd1–N1 172.2(2)°, C21–Pd1–N1 105.02(17)°, N2–Pd1–N1 80.33(13)°.

secondary amine bridge, which altogether suggested that these complexes were much more acidic than expected. According to ^{13}C-APT NMR (Fig. S2, S4, S6 and S8, ESI†), the ligands **H_2L^1** and **H_2L^2** have six quaternary carbon peaks, while their palladium complexes have seven, thus demonstrating that cyclometallation did occur. Altogether **PdL^1** and **PdL^2** appear to be neutral complexes; their identical HRMS data also demonstrated they are coordination isomers.

Vapor diffusion of diethyl ether into a methanol solution of **PdL^2** yielded red rectangular crystals suitable for X-ray structure determination (Table S1, ESI,† and Scheme 1b). **PdL^2** crystallized in the centrosymmetric $P2_1/n$ monoclinic space group. Three nitrogen and one carbon atom were coordinated to the palladium(II) cation, with bond lengths in the range 1.988(3)–2.028(4) Å for the three Pd–N bonds, and a Pd–C bond distance of 2.017(4) Å. The coordination sphere was slightly distorted, with a dihedral angle N1–N2–N4–C21 of 2.33°. τ_4, a structural parameter calculated by $(360° - (\alpha + \beta))/(141°)$, where α and β are the two greatest valence angles of the coordination sphere,[31] was 0.093 in the structure of **PdL^2**, which is typical of an essentially square planar complex. Deprotonation of the nitrogen bridge was evident from the shorter distance between the amine nitrogen atoms and the adjacent pyridine carbon atoms (C10–N3 = 1.353(4) Å and C11–N3 = 1.349(4) Å), compared to that found in metal complexes with protonated nitrogen bridges (N–C distances in the range 1.36 Å to 1.39 Å).[29,30] Also, unlike for [Fe(Hbbpya)(NCS)$_2$],[32] no residual electron density was found near the bridging N atom in the structure of **PdL^2**. Finally, the asymmetric unit contained no counter-ions. In summary, single crystal X-ray crystallography is consistent with NMR and IR data, showing that **PdL^1** and **PdL^2** are neutral species because deprotonation of the nitrogen bridge becomes very easy upon coordination.

The absorption spectrum of both complexes in PBS : DMSO (1 : 1) solution at 310 K (Fig. S10, ESI†) presented no significant changes over 24 hours, suggesting that the complexes were thermally stable under such conditions. Similar results were obtained in cell-growing medium (Fig. S11, ESI†), demonstrating good stability under such conditions. The partition coefficients ($\log P_{ow}$) of the palladium complexes were determined by the shake-flask method (Table S2, ESI†). $\log P_{ow}$ was lower for **PdL^1** (−0.64) than for **PdL^2** (+0.046), confirming the higher solubility in water of the former, compared to the latter. Their cytotoxicity was tested in lung (A549) and skin (A431) cancer cell lines, both in the dark and upon blue light activation. Low doses of blue light were chosen (455 nm, 5 min, 10.5 mW cm^{-2}, 3.2 J cm^{-2}) which have by themselves no effect on cell growth.[33] The cell growth inhibition effective concentrations (EC_{50}) of **PdL^1** and **PdL^2** are reported in Table 1, and the dose–response curves are shown in Fig. 1 and Fig. S12 (ESI†). In the dark both compounds showed significant anticancer activity, with an EC_{50} around 10 μM for **PdL^1** and **PdL^2** in A549 cells, respectively. After blue light activation, **PdL^1** showed a notable 13- or 4.0-fold increase in cytotoxicity in A549 and A431, respectively, while **PdL^2** showed a negligible photoindex of 1.3 or 1.4, respectively. The difference in photocytotoxicity between the two coordination isomers was quite intriguing. To investigate the reason for such a difference, we first measured the singlet oxygen ($^1O_2$) generation quantum yield (φ_Δ) of these two isomers in CD_3OD spectroscopically. φ_Δ was more than twice higher for **PdL^1** (0.89) than for **PdL^2** (0.38, Fig. 2b and Table S3, ESI†), and higher than the reference $[Ru(bpy)_3]Cl_2$ (0.73).[34] However, **PdL^2** was still a decent $^1O_2$ generator. In methanol, the absorbance spectra of both complexes (Fig. 2) were similar in the 270–300 nm region; however, **PdL^1** had a much higher absorption in the blue region with λ_{max}^{abs} = 422 nm, compared to **PdL^2** that absorbed in the near-UV region (λ_{max}^{abs} = 347 nm). In this solvent the molar absorptivity at 455 nm for **PdL^1** and

Table 1 The cell growing inhibition effective concentrations (EC_{50} in μM) of **PdL^1** and **PdL^2** towards A549 and A431 human cancer cell lines. 95% confidence interval (CI in μM) and photoindex (PI = EC_{50}, dark/EC_{50}, light) are also indicated

		EC_{50} (μM)			
Complexes		A549	±CI	A431	±CI
PdL^1	Dark	12	+3.0 −3.0	20	+4.0 −3.0
	Light	0.9	+0.8 −0.5	5.0	+2.0 −1.0
PI		13		4.0	
PdL^2	Dark	8.0	+2.0 −1.0	14	+2.0 −1.0
	Light	6.0	+0.8 −0.7	10	+1.0 −1.0
PI		1.3		1.4	

Irradiation condition: 455 nm blue light, 5 min, 10.5 mW cm^{-2}, 3.2 J cm^{-2}. Data is the mean over three independent experiments.

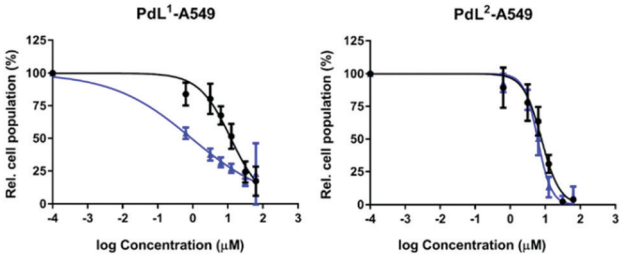

Fig. 1 Dose–response curves for A549 cells incubated with palladium complexes and irradiated 5 min with blue light (blue data points), or in the dark (black data points).

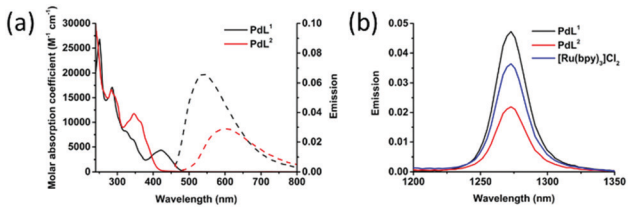

Fig. 2 (a) The molar absorption coefficient (solid line) and emission spectra (dashed line) of **PdL^1** (black), **PdL^2** (red) in CH_3OH. (b) Singlet oxygen emission spectra of $[Ru(bpy)_3]Cl_2$ (blue), **PdL^1** (black), **PdL^2** (red) in CD_3OD irradiated with blue light (λ_{ex} = 450 nm, 50 mW, 0.4 W cm^{-2}).

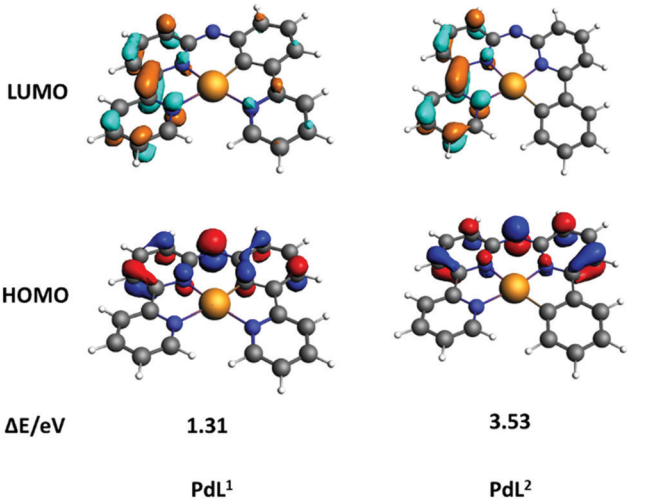

Fig. 3 DFT calculation of HOMOs (bottom) and LUMOs (top) orbitals of **PdL^1** and **PdL^2**; occupied orbitals (HOMO) have red and blue lobes, and unoccupied orbitals (LUMO) brown and cyan lobes. Element colour code: grey = C; orange = Pd; blue = N; white = H.

PdL^2 was 2004 M^{-1} cm^{-1} and 133 M^{-1} cm^{-1}, respectively, indicating a 15-fold enhanced absorption of **PdL^1** in the blue region, compared with **PdL^2**. Considering their similar lifetime (0.271 *vs.* 0.333 ns for the main component of their biexponential decay, Table S3 and Fig. S13, ESI†), the difference in $^1O_2$ generation efficiency is probably a consequence of the higher phosphorescence quantum yield for **PdL^1** (0.0017) *vs.* **PdL^2** (0.00084, Table S3, ESI†), which points to the slower non-radiative decay pathways for the former, compared to the latter. Altogether, the dramatically higher phototoxicity of **PdL^1**, compared to **PdL^2**, seems to result from the much better absorption of blue light of **PdL^1**, coupled to its higher phosphorescence quantum yield, which leads to higher $^1O_2$ generation efficiency. Although different log P_{ow} values may lead to different cell uptake and sub-cellular localization for both isomers as well, the better photobiological properties of **PdL^1** depend, at least in part, on the much better photodynamic properties of **PdL^1** (ε_{455} and φ_Δ), compared to its isomer **PdL^2**.

Density functional theory (DFT) calculations were performed to understand why **PdL^1** exhibited higher absorption in the blue domain than its isomer **PdL^2**. The nature of the highest occupied molecular orbital (HOMO) and lowest unoccupied molecular orbitals (LUMO) is highly relevant to predict the photophysical properties of metal complexes.[34–36] As showed in Fig. 3, the HOMO and LUMO orbitals of both isomers **PdL^1** and **PdL^2** had π symmetry and were centered on the ligand, with a negligible contribution of the palladium(II) center. The bridged secondary amine is the major contributor to the HOMO of both palladium complexes, attributing for 20.4 (**PdL^1**) and 21.8% (**PdL^2**) of the electron density. The rest of the HOMO orbital density was located in the aromatic rings directly connected to the nitrogen bridge. By contrast, the LUMO orbitals for both complexes were centered on the bipyridyl fragment. This suggested that the lowest energy absorption band of both palladium complexes should be of ligand-to-ligand charge transfer character, from the amine to the bipyridyl.

The calculated energies of HOMOs, LUMOs and energy gaps are listed in Table S4 (ESI†). The HOMO of **PdL^1** was significantly higher in energy than that of **PdL^2**, indicating the higher electron-donating effect of the negatively charged carbon atom of **PdL^1**, compared with that of **PdL^2** which is further away from the nitrogen bridge. By contrast, the LUMO energy levels of both palladium complexes were similar, because LUMO orbitals are located on the almost equivalent bipyridyl fragments. Such lower energy gap of **PdL^1** suggested better absorption of low-energy light, which explains the observed differences in the UV-vis spectra of the two isomers. These results were confirmed by time-dependent density functional theory calculations (TDDFT) for both complexes in methanol, using COSMO to simulate solvent effects (Fig. S14, ESI,† left). The calculated spectrum of **PdL^1** (Fig. S14, ESI,† left) showed a lower energy (515 nm) for the HOMO–LUMO transition, compared to **PdL^2** (449 nm). These transition energies were increased (404 and 367 nm, respectively) by protonation of the nitrogen bridge (Fig. S14, ESI,† right), which may happen in the slightly acidic environment of cancer cells; however, the trend between $[Pd(HL^1)]^+$ and $[Pd(HL^2)]^+$ was identical to that seen for **PdL^1** and **PdL^2**. Overall, calculations clearly demonstrated that a change of the position of the carbon–metal bond had a strong influence on the HOMO–LUMO energy gaps of these cyclometallated palladium complexes.

In summary, the new cyclopalladated complex **PdL^1** showed good absorbance in the blue region of the spectrum, low phosphorescence, and excellent singlet oxygen quantum yield (0.89), which altogether translated into high photoindex in human cancer cells. By contrast, its isomer **PdL^2** had low absorption and low singlet oxygen quantum yield (0.38), resulting in negligible activation by blue light *in vitro*. DFT calculation showed that the higher absorption in the blue region of **PdL^1**, and thus its lower HOMO–LOMO energy gap, was due to the closer proximity between the electron-rich cyclometallated aromatic cycle and the nitrogen bridge of the ligand, while in **PdL^2** both aromatic rings adjacent to the N bridge are electron-poor pyridine rings, which lowers the HOMO energy level. To the best of our knowledge, this study is the first report that two isomers of organometallic prodrugs have different photobiological properties. These results demonstrate that changing the position of the carbon–metal bond in the coordination sphere of photoactive organometallic prodrugs can be used to tune the energy gap between their frontier orbitals, and hence their absorption in the visible region of the spectrum.

X. Zhou gratefully acknowledges the China Scholarship Council (CSC) for a personal grant (No. 201606200045). This work is supported by an ERC Starting Grant to S. Bonnet.

Conflicts of interest

There are no conflicts to declare.

Notes and references

1 T. C. Johnstone, K. Suntharalingam and S. J. Lippard, *Chem. Rev.*, 2016, **116**, 3436–3486.
2 L. Kelland, *Nat. Rev. Cancer*, 2007, **7**, 573–584.
3 D. Wang and S. J. Lippard, *Nat. Rev. Drug Discovery*, 2005, **4**, 307–320.
4 L. Ma, N. Wang, R. Ma, C. Li, Z. Xu, M. K. Tse and G. Zhu, *Angew. Chem., Int. Ed.*, 2018, **57**, 1–6.
5 S. Medici, M. Peana, V. M. Nurchi, J. I. Lachowicz, G. Crisponi and M. A. Zoroddu, *Coord. Chem. Rev.*, 2015, **284**, 329–350.
6 N. Cutillas, G. S. Yellol, C. de Haro, C. Vicente, V. Rodriguez and J. Ruiz, *Coord. Chem. Rev.*, 2013, **257**, 2784–2797.
7 L. Zeng, P. Gupta, Y. Chen, E. Wang, L. Ji, H. Chao and Z. S. Chen, *Chem. Soc. Rev.*, 2017, **46**, 5771–5804.
8 F. E. Poynton, S. A. Bright, S. Blasco, D. C. Williams, J. M. Kelly and T. Gunnlaugsson, *Chem. Soc. Rev.*, 2017, **46**, 7706–7756.
9 H. Huang, P. Zhang, H. Chen, L. Ji and H. Chao, *Chem. – Eur. J.*, 2015, **21**, 715–725.
10 T. T. Fong, C. N. Lok, C. Y. Chung, Y. M. Fung, P. K. Chow, P. K. Wan and C. M. Che, *Angew. Chem., Int. Ed.*, 2016, **55**, 11935–11939.
11 M. Fanelli, M. Formica, V. Fusi, L. Giorgi, M. Micheloni and P. Paoli, *Coord. Chem. Rev.*, 2016, **310**, 41–79.
12 A.-R. Azzouzi, S. Vincendeau, E. Barret, A. Cicco, F. Kleinclauss, H. G. van der Poel, C. G. Stief, J. Rassweiler, G. Salomon, E. Solsona, A. Alcaraz, T. T. Tammela, D. J. Rosario, F. Gomez-Veiga, G. Ahlgren, F. Benzaghou, B. Gaillac, B. Amzal, F. M. J. Debruyne, G. Fromont, C. Gratzke and M. Emberton, *Lancet Oncol.*, 2017, **18**, 181–191.
13 H. Cao, L. Wang, Y. Yang, J. Li, Y. Qi, Y. Li, Y. Li, H. Wang and J. Li, *Angew. Chem., Int. Ed.*, 2018, **57**, 7759–7763.
14 Y. Ma, X. Li, A. Li, P. Yang, C. Zhang and B. Tang, *Angew. Chem., Int. Ed.*, 2017, **56**, 13752–13756.
15 S. H. Askes, A. Bahreman and S. Bonnet, *Angew. Chem., Int. Ed.*, 2014, **53**, 1029–1033.
16 S. L. Higgins and K. J. Brewer, *Angew. Chem., Int. Ed.*, 2012, **51**, 11420–11422.
17 H. Bi, Y. Dai, P. Yang, J. Xu, D. Yang, S. Gai, F. He, B. Liu, C. Zhong, G. An and J. Lin, *Small*, 2018, **14**, e1703809.
18 H. Bi, Y. Dai, P. Yang, J. Xu, D. Yang, S. Gai, F. He, G. An, C. Zhong and J. Lin, *Chem. Eng. J.*, 2019, **356**, 543–553.
19 J. D. Knoll and C. Turro, *Coord. Chem. Rev.*, 2015, **282-283**, 110–126.
20 F. Heinemann, J. Karges and G. Gasser, *Acc. Chem. Res.*, 2017, **50**, 2727–2736.
21 J.-Y. Lee, J.-Y. Lee, Y.-Y. Chang, C.-H. Hu, N. M. Wang and H. M. Lee, *Organometallics*, 2015, **34**, 4359–4368.
22 S. Ray, R. Mohan, J. K. Singh, M. K. Samantaray, M. M. Shaikh, D. Panda and P. Ghosh, *J. Am. Chem. Soc.*, 2007, 15042–15053.
23 S. G. Churusova, D. V. Aleksanyan, E. Y. Rybalkina, O. Y. Susova, V. V. Brunova, R. R. Aysin, Y. V. Nelyubina, A. S. Peregudov, E. I. Gutsul, Z. S. Klemenkova and V. A. Kozlov, *Inorg. Chem.*, 2017, **56**, 9834–9850.
24 W. Liu and R. Gust, *Chem. Soc. Rev.*, 2013, **42**, 755–773.
25 J. Ruiz, V. Rodriguez, C. de Haro, A. Espinosa, J. Perez and C. Janiak, *Dalton Trans.*, 2010, **39**, 3290–3301.
26 G. Gasser, I. Ott and N. Metzler-Nolte, *J. Med. Chem.*, 2011, **54**, 3–25.
27 S. Bonnet, *Comments Inorg. Chem.*, 2014, **35**, 179–213.
28 Z. Fan, J. Ni and A. Zhang, *J. Am. Chem. Soc.*, 2016, **138**, 8470–8475.
29 V. H. S. van Rixel, B. Siewert, S. L. Hopkins, S. H. C. Askes, A. Busemann, M. A. Siegler and S. Bonnet, *Chem. Sci.*, 2016, **7**, 4922–4929.
30 E. M. Hernández, S. Zheng, H. J. Shepherd, D. S. Yufit, K. Ridier, S. Bedoui, W. Nicolazzi, V. Velázquez, S. Bonnet, G. Molnár and A. Bousseksou, *J. Phys. Chem. C*, 2016, **120**, 27608–27617.
31 L. Yang, D. R. Powell and R. P. Houser, *Dalton Trans.*, 2007, 955–964.
32 S. Zheng, N. R. Reintjens, M. A. Siegler, O. Roubeau, E. Bouwman, A. Rudavskyi, R. W. Havenith and S. Bonnet, *Chem. – Eur. J.*, 2016, **22**, 331–339.
33 S. L. Hopkins, B. Siewert, S. H. Askes, P. Veldhuizen, R. Zwier, M. Heger and S. Bonnet, *Photochem. Photobiol. Sci.*, 2016, **15**, 644–653.
34 X. Li, J. Zhang, Z. Zhao, L. Wang, H. Yang, Q. Chang, N. Jiang, Z. Liu, Z. Bian, W. Liu, Z. Lu and C. Huang, *Adv. Mater.*, 2018, **30**, e1705005.
35 F. F. Hung, S. X. Wu, W. P. To, W. L. Kwong, X. Guan, W. Lu, K. H. Low and C. M. Che, *Chem. – Asian J.*, 2017, **12**, 145–158.
36 J. Fernandez-Cestau, B. t. Bertrand, A. Pintus and M. Bochmann, *Organometallics*, 2017, **36**, 3304–3312.

